

Article

# Simultaneous Selective Chlorination and Carbothermic Reduction of High-Iron Manganese Ore for the Recovery of Manganese Chloride and Metallic Iron

Dawei Yu , Fuhui Cui , Yunxiang Cong, Chunxi Zhang, Qinghua Tian and Xueyi Guo \*

School of Metallurgy and Environment, Central South University, 932 Lushan South Road, Changsha 410083, China; fuhuicui@csu.edu.cn (F.C.); sdcyxiang@163.com (Y.C.); zhangchunxi@csu.edu.cn (C.Z.); qinghua@csu.edu.cn (Q.T.)

\* Correspondence: dawei.yu@csu.edu.cn (D.Y.); xyguo@csu.edu.cn (X.G.); Tel.: +86-0731-88876255 (D.Y.)

Received: 10 September 2019; Accepted: 18 October 2019; Published: 20 October 2019



**Abstract:** Metallurgical processing of low-grade manganese ore with high iron content is gaining increasing attention due to the gradual depletion of high-grade Mn ores, amid the difficulties in its efficient extraction for both Mn and Fe values in an environmentally-friendly manner. Attempting to tackle the difficulties, this paper describes an innovative process for selectively chlorinating and reducing the high-Fe manganese ore in a simultaneous manner, aiming to produce water-soluble  $\text{MnCl}_2$  and metallic Fe. After pre-mixing with carbonaceous reductant,  $\text{CaCl}_2$  and  $\text{MgCl}_2$  as the chlorinating agent, the Mn ore was heated at 1000 °C. As much as 89.4% Mn can be chlorinated in its water-soluble form, with dissolution of only 3.0% Fe. The presence of  $\text{CaCl}_2$  during carbothermic reduction resulted in significant promotion in both the Fe reduction rate and formation of large metallic Fe particles due to the segregation effect, facilitating subsequent separation. Selective Mn chlorination by  $\text{MgCl}_2$  took place with or without the involvement of  $\text{SiO}_2$ , forming  $\text{MgSiO}_4$  or  $\text{MgO}$ , respectively.

**Keywords:** manganese ore; chlorination; carbothermic reduction; manganese chloride; segregation

## 1. Introduction

Manganese has been a critical element for the production of steels, batteries, fertilizer, non-ferrous alloys, catalysts, and pigment, etc. [1–3] Driven by the high crude steel production rate of China, global manganese resources have been mostly consumed by the country [4,5] for the production of manganese ferroalloy, which is produced by smelting with submerged electric arc furnaces (SAF) at a high energy cost [6–9]. Cheap and high-grade manganese ores have become scarce due to its continuous consumption. Increasing attention has therefore been given to the development of technically and economically viable technologies for the utilization of medium- and low-grade manganese ores [10–12]. In addition, large quantities of manganese ore fines and tailings have been generated due to ineffective recovery technology and selective mining of high grade manganese ores [12–14], necessitating further treatment for metal recovery.

Low grade manganese ores (<40%) generally contain typical impurity elements such as Fe, Al, and Si, etc. [15] They are conventionally processed by initial reductive roasting or melting followed by treating with hydrometallurgical approaches for the production of chemical manganese dioxide, electrolytic manganese, or electrolytic manganese dioxide [11,16]. The purpose of reductive roasting is to reduce the manganese oxides to low-valence state (i.e.,  $\text{Mn}^{2+}$ ), which becomes soluble in dilute acids [17], allowing for subsequent hydrometallurgical processing. Various reductants (e.g.,

charcoal [18], straw [19,20], saw dust [20], bamboo [20], wheat stalk [20,21], bagasse [22], cornstalk [23], and sulfur [17], etc.) have been studied for the reduction of manganese ore followed by leaching with acid. Impurities (such as Fe) can be co-leached [15], resulting in the generation of large quantities of residues during the subsequent hydrometallurgical purification steps. In this process, iron is not recovered in a useful form, and it leads to the formation of residues which can be problematic when disposed to the environment.

Manganese ores with high content of Fe are generally not suitable for the production of manganese ferroalloys [1,24]. Upgrading the manganese ores by iron removal using mineral beneficiation is inefficient [25], due to the complex mineral nature and high similarities in density and magnetic susceptibility of manganese and its associated iron minerals [4]. Attempts have therefore been made to amplify the difference between Mn- and Fe-bearing phases in terms of their magnetic susceptibility, by selective thermal reduction of iron oxides to form strongly magnetic  $\text{Fe}_3\text{O}_4$  [24,26,27]. Upgrading the manganese ores by iron removal can be realized by subsequent magnetic separation. This approach generally suffers from the following drawbacks: (1) Mn loss is high at a high degree of iron removal; (2) Fe is not recovered in a useful form; (3) This thermal upgrading step adds to the complexity of the existing processes, and potentially increases the overall energy cost.

In efforts to address the above-mentioned issues, the current study aims at developing an efficient and environmentally-friendly process for the extraction of both Mn and Fe from the high-iron manganese ores. Calcium chloride ( $\text{CaCl}_2$ ) has been proven to be an effective agent that not only accelerates the carbothermic reduction, but also promotes the formation of individual ferrochromium alloy particles during carbothermic segregation reduction of chromite, allowing for easier physical separation of the ferrochromium from other gangue minerals [28,29]. In the current study,  $\text{CaCl}_2$  was also employed as the segregation agent that promotes carbothermic reduction of high-iron manganese ore, aiming for the selective reduction of iron oxides to their metallic form (i.e.,  $\text{Fe}^0$ ). In addition, magnesium chloride ( $\text{MgCl}_2$ ) was employed as the chlorination agent that will selectively chlorinate the manganese oxides, producing  $\text{MnCl}_2$ . Selective carbothermic reduction and chlorination takes place simultaneously, resulting in the formation of metallic Fe and water-soluble  $\text{MnCl}_2$ . Therefore, Mn can be recovered in the form of  $\text{MnCl}_2$  by water-leaching the product, and Fe can be recovered in its metallic form by magnetic separation of the water-leach residue.

### *Thermodynamic Considerations*

Thermodynamic basis for the simultaneous selective carbothermic reduction and chlorination of high-iron manganese ores can be illustrated by Figure 1. This figure is produced using the thermodynamic data produced from the thermochemical software HSC Chemistry 6.12 [30]. For the carbothermic reduction in the presence of solid carbon, the equilibrium partial pressure of CO is dependent on the reduction temperature, which is governed by the Boudouard reaction (Equation (1)) [31], as seen from Figure 1a. This determines the reduction products of iron oxides and manganese oxides at equilibrium conditions (i.e.,  $\text{Fe}_3\text{O}_4$  at temperatures below 650 °C; FeO at 650–690 °C; metallic Fe at temperatures above 690 °C; MnO at temperatures below 1400 °C; and metallic Mn at temperatures above 1400 °C). Therefore, carbothermic reduction of high-iron manganese oxides can result in the formation of metallic Fe and MnO in the temperature range of 690–1400 °C, providing the thermodynamic basis for the selective metallization of iron species.

Figure 1b exhibits the equilibrium constants for the main possible chlorination reactions when using  $\text{MgCl}_2$  as the chlorination agent. The superimposed (Mn, Fe, Mg, Ca)-Cl-O predominance area diagram at 1000 °C is shown in Figure 1c. As seen from both figures, MnO generated from carbothermic reduction (Figure 1a) can be further chlorinated by  $\text{MgCl}_2$  (Equation (2)).  $\text{SiO}_2$  and  $\text{Al}_2\text{O}_3$  (main components of the gangue minerals) cannot be chlorinated by  $\text{MgCl}_2$ , revealed by the extremely low equilibrium constants for their corresponding chlorination reactions (Figure 1b). FeO generated from the step-wise carbothermic reduction of iron oxides [32] could also be chlorinated by  $\text{MgCl}_2$ , forming  $\text{FeCl}_2$  (Equation (3)). Fortunately,  $\text{FeCl}_2$  can be consumed by reacting further with MnO

(Figure 1b,c), represented by Equation (4). FeO regenerated from this reaction would be subsequently reduced to metallic Fe at temperatures higher than 690 °C, as seen from Figure 1a. Therefore, by coupling chlorination with carbothermic reduction reactions, it is thermodynamically feasible to achieve selective chlorination of MnO and selective metallization of Fe species in a simultaneous manner. This window of opportunity for simultaneous selective chlorination of MnO and metallization of Fe species at 1000 °C is shown as the highlighted predominance area (in yellow) in Figure 1c. It can also be revealed from Figure 1c that using CaCl<sub>2</sub> as the chlorinating agent is not effective in achieving selective chlorination, compared to MgCl<sub>2</sub>.

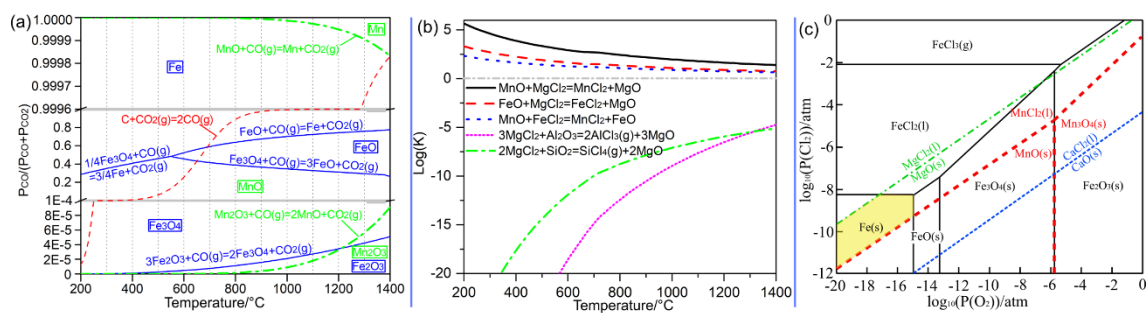


**Figure 1.** (a) Stability diagram for the superimposed Fe–O (solid blue lines) and Mn–O (dash-dotted green lines) systems under CO–CO<sub>2</sub> atmospheres, and CO partial pressure established by the Boudouard reaction (dashed red line). Please note the horizontal grey lines indicates the change of scales for the *y*-axis. (b) Equilibrium constants (in logarithmic form) for the main chlorination reactions as a function of temperature. (c) Superimposed (Mn, Fe, Mg, Ca)–Cl–O predominance area diagram at 1000 °C showing the window of opportunity (highlighted in yellow) for simultaneous selective chlorination of MnO and metallization of Fe species.

## 2. Materials and Methods

### 2.1. Materials

The low grade high-iron manganese ore used in the study was produced in Zambia after hand-picking and removal of high-quality ores. The low-grade ore was crushed, grinded and sieved, after which the size fraction of 30–150 μm was used for the investigation. Graphite powders (99.95% pure) in the particle size range of 45–150 μm were used as the carbothermic reductant. Anhydrous MgCl<sub>2</sub> (99.9% pure) and CaCl<sub>2</sub> (99.9% pure) in their fine powder form were used as additives.

### 2.2. Experimental Procedure

As illustrated by Figure 2, for each experiment, 5.0 g Mn ore powders were mixed with 0.9 g graphite and varying proportions of CaCl<sub>2</sub> and MgCl<sub>2</sub> powders, before placing into a graphite crucible (#8, O.D. 30 mm, I.D. 22 mm, height 40 mm) and covered with a graphite lid. Five small holes were drilled on the lid beforehand, to allow escape of the gas evolved from the reactions during the experiment. The graphite crucible was placed into a long quartz crucible (#7, O.D. 39 mm, I.D. 35 mm, height 340 mm). Subsequently, twenty thin quartz tubes (#6, O.D. 5 mm, I.D. 2.9 mm, length 300 mm) were placed on top of the graphite lid inside the long quartz crucible, for the condensation of chloride vapors. The long quartz crucible was subsequently loaded into the vertical tube furnace (#3), supported

by a porous quartz frit (#5) so that the graphite crucible was situated at the center of the heating zone. With a continuous flow of 50 mL/min Ar gas (5N), the sample mixture was heated to 1000 °C at a heating rate of 15 °C/min, and dwelled at 1000 °C for a predetermined time before cooling to room temperature at a cooling rate of 15 °C/min. A scrubber bottle (#11) containing 500 mL deionized water was used to capture residual chloride vapors from the evolved gas.

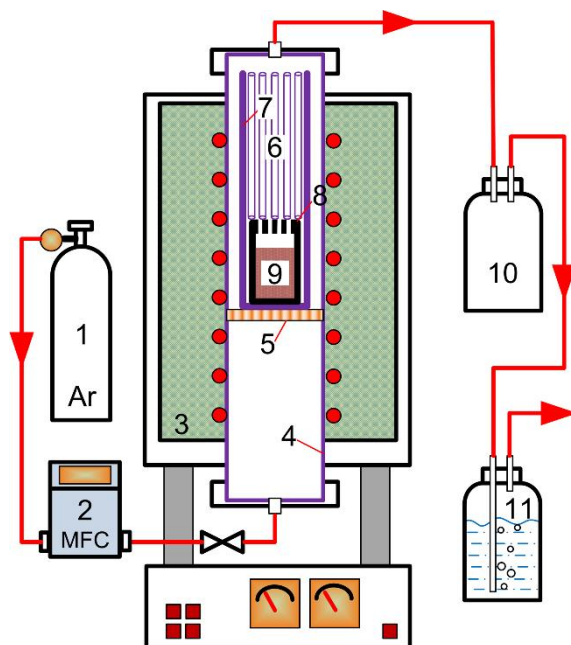


**Figure 2.** Schematic illustration of the experimental setup (1. Ar gas; 2. Mass flow controller; 3. Electric tube furnace; 4. Quartz tube; 5. Porous frit; 6. Thin quartz tubes for condensation; 7. Long quartz crucible; 8. Graphite crucible with lid (with five holes); 9. Sample mixture; 10. Buffer bottle; 11. Scrubber).

Chlorination leads to the formation of water-soluble chlorides, some of which were evaporated and condensed on the thin quartz tubes and the inner wall of the long quartz crucible (#6 and #7 in Figure 2, respectively). To quantify this, 3.0 g of sample product was leached with 100 mL deionized water at 50 °C for 60 min. After filtration, the leach solution (L1) was sampled for wet chemical analysis. The leach residue (R1) was dried in an oven at 110 °C for 120 min. Chemical composition of R1 was analyzed by fusion with NaOH at 700 °C to allow subsequent complete digestion with HCl solution before wet chemical analysis. The thin quartz tubes were placed into the long quartz crucible filled with deionized water, which was heated with a water bath at 50 °C for 60 min. The resulting solution (L2) and the solution in the scrubber (L3) were also taken for wet chemical analysis. The degree of chlorination for each element was calculated according to Equation (5), based on wet chemical analysis of all samples mentioned above. The degree of evaporation of chlorides was calculated based on Equation (6).

$$\text{Chlorination degree} = \frac{m_{\text{sol}} + m_{\text{con}} + m_{\text{scr}}}{m_{\text{insol}} + m_{\text{sol}} + m_{\text{con}} + m_{\text{scr}}} \times 100\% \quad (5)$$

where  $m_{\text{sol}}$ ,  $m_{\text{insol}}$ ,  $m_{\text{con}}$ , and  $m_{\text{scr}}$  represent the mass of each element in water-soluble and water-insoluble forms in the sample product, in condensed form, and in the scrubber solution, respectively.

$$\text{Evaporation degree} = \frac{m_{\text{con}} + m_{\text{scr}}}{m_{\text{sol}} + m_{\text{con}} + m_{\text{scr}}} \times 100\% \quad (6)$$

### 2.3. Analytical Methods

Wet chemical analysis was performed using inductively coupled plasma optical emission spectrometry (ICP-OES, Spectro Blue SOP, Kleve, Germany) for the concentrations of Mn, Fe, Mg, and Ca, after proper dilution of each liquid sample. The dilution resulted in the elemental concentrations of less than 50 mg/L before analysis by ICP-OES. For each element, three calibration lines were firstly created using standard solutions, corresponding to the concentration ranges of 0–1, 1–10 and 10–50 mg/L. Each analysis of the liquid sample lasted for 30 s, and was repeated three times. Based on the concentration range of the element, its corresponding calibration line was applied. The average of the three repeated analyses was reported as the final result. The detection limits are 0.1, 0.4, 0.01, and 0.1 µg/L for Mn, Fe, Mg, and Ca, respectively. Relative standard deviation (RSD) was <2% for the analysis. Chemical composition of the original manganese ore for Mn, Fe, Al, Si, Ba, Ca, Mg, Na, K, and Pb was analyzed using China National Standards (listed in the Supplementary Material). Loss on ignition (LOI) of the manganese ore was conducted using a sample size of 1 g by heating in air at 950 °C for 2 h. Sample weight after the first and second hour was recorded and compared, making sure a constant weight was reached. The dried residue after water-leaching was mounted into epoxy resin, grinded with sand papers, and polished with diamond suspension to prepare the polished section. It was analyzed with scanning electron microscopy (SEM, TESCAN MIRA3, Tescan, Kohoutovice, Czech Republic) coupled with energy dispersive spectroscopy (EDS, Oxford XMAX20, Oxford Instruments, Abingdon, UK), using an accelerating voltage of 20 kV. For qualitative phase identification, solid samples were firstly grinded with mortar and pestle for approximately 15 min to ensure they are in fine powder form before analysis by X-ray powder diffraction (XRD, Rigaku 3014Z, Rigaku, Tokyo, Japan) with Cu K $\alpha$  radiation at 40 kV, 200 mA.

## 3. Results and Discussion

### 3.1. Characterization of the Mn Ore

Chemical composition of the Mn ore and its XRD pattern are shown in Table 1 and Figure 3, respectively. As seen, the ore has a high Fe content of 40.54 wt%, and a low Mn/Fe mass ratio of 0.34. The main minerals are bixbyite (Mn, Fe) $_2$ O $_3$ , hematite Fe $_2$ O $_3$ , and quartz SiO $_2$ . Back scattered electron (BSE) image and its elemental mappings of the cross section of the ore are exhibited in Figure 4, indicating that the three main minerals are generally well liberated. As the main Mn-bearing mineral in the ore, bixbyite contains only minor amounts of Fe. Based on energy dispersive spectroscopy (EDS) analysis, the Mn/Fe mass ratio of bixbyite is approximately 10:1.

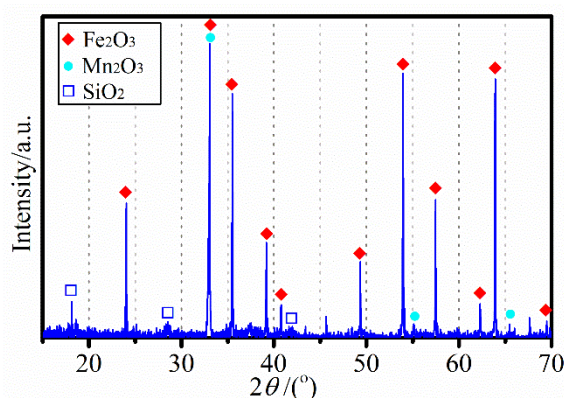
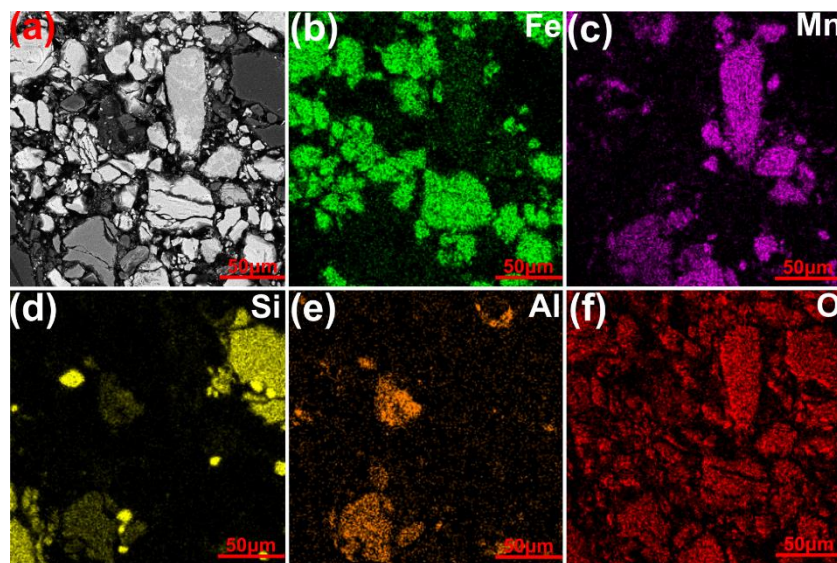


Figure 3. XRD (X-ray powder diffraction) pattern of the high-iron manganese ore used in the study.



**Figure 4.** BSE (Back scattered electron) image (a) and elemental mapping (b–f) of the high-iron manganese ore.

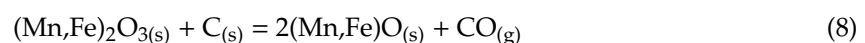
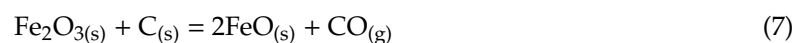
**Table 1.** Chemical composition of the manganese ore (wt%).

Total Fe	Total Mn	SiO <sub>2</sub>	Al <sub>2</sub> O <sub>3</sub>	CaO	MgO	BaO	K <sub>2</sub> O	Na <sub>2</sub> O	PbO	LOI *
40.54	13.86	7.14	2.57	0.18	0.18	1.17	0.30	0.04	0.02	3.41

\* LOI: loss on ignition.

### 3.2. Carbothermic Reduction without Additives

High-iron manganese ore was reduced at 1000 °C for 1, 2 and 4 h without the addition of CaCl<sub>2</sub> and MgCl<sub>2</sub>. XRD patterns and SEM analysis of the reduced products are shown in Figures 5 and 6, respectively. As seen, carbothermic reduction of the manganese ore was slow. After reduction for 1 h, partial reduction of hematite and bixbyite took place, forming their respective monoxides (i.e., FeO and (Mn, Fe)O), which can be represented by Equations (7) and (8). An Fe-rich metallic phase was identified from the product after 2 h reduction (Figure 5b), which was produced from further reduction of monoxide FeO (Equation (9)). This metallic phase fits best with Fe<sub>19</sub>Mn (PDF card# 03-065-7528). However, it generally contains no more than 2 wt% Mn based on EDS analysis. The XRD peaks for metallic Fe became higher after 4 h reduction (Figure 5c), indicating a high reduction degree. With the progress of reduction, the FeO peak at 42° shifted towards left, which is highlighted and re-plotted as an inset in Figure 5. This reflected its compositional change towards Mn- and Fe-bearing monoxides (Fe, Mn)O with an increasing Mn/Fe ratio, which could possibly be due to the continuous consumption of FeO by reduction (Equation (9)) and the reaction between FeO and MnO forming the monoxide solid solution (Fe, Mn)O. As seen from Figure 6b, quartz (SiO<sub>2</sub>) also gradually reacted with other adjacent oxides, such as FeO, (Mn, Fe)O and Al<sub>2</sub>O<sub>3</sub>, forming the core-shell structure with the core being SiO<sub>2</sub>. Some (Mn, Fe)O particles started to develop a porous shell containing lower concentrations of Fe and high concentrations of Si (approximately 13 wt% based on EDS analysis), possibly due to the preferential reduction of Fe species on the surface of the particle leading to volume shrinkage. In general, the selective reduction of iron oxides was slow, reflected by the presence of Fe-bearing monoxide solid solution even after 4 h reduction.



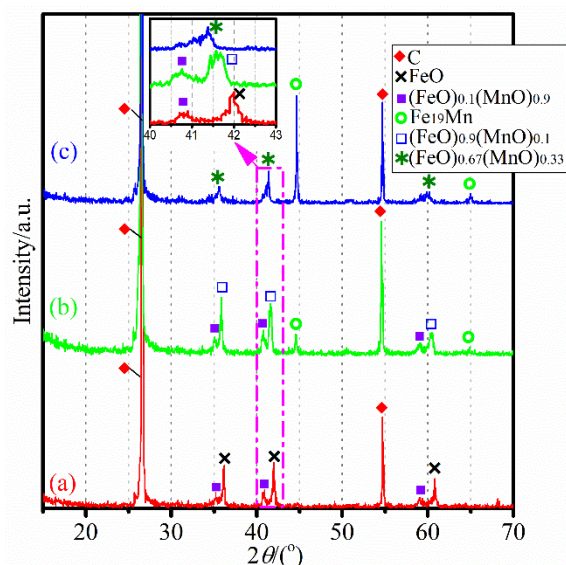


Figure 5. XRD patterns of the samples collected after reduction at 1000 °C for (a) 1 h, (b) 2 h, and (c) 4 h.

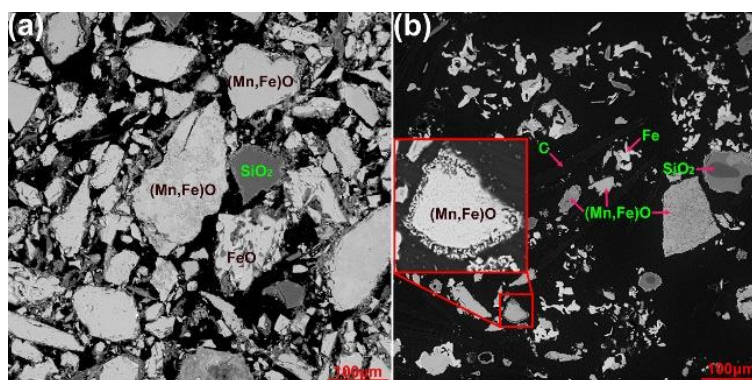
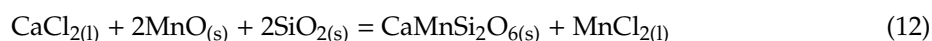
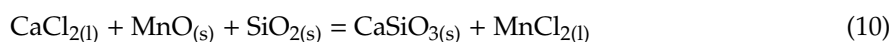
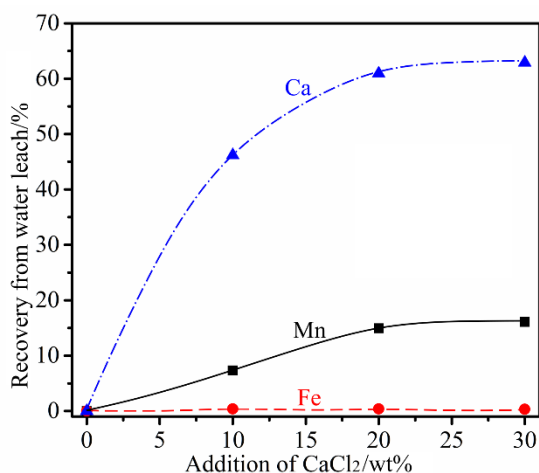


Figure 6. BSE images of the sample products collected after reduction at 1000 °C for (a) 2 h and (b) 4 h.

### 3.3. Influence of $\text{CaCl}_2$ Addition

Carbothermic reduction of high-Fe manganese ore was conducted at 1000 °C for 2 h in the presence of varying amounts of  $\text{CaCl}_2$  (0–30 wt% of ore). Recovery of metals by water-leaching was plotted in Figure 7. Residues produced from water-leaching were further analyzed by XRD, with their patterns shown in Figure 8. The Ca curve in Figure 7 suggests that  $\text{CaCl}_2$  partially reacted with the ore, resulting in the incomplete dissolution of Ca during water-leaching due to the formation of water-insoluble Ca-bearing compounds. These compounds were identified as  $\text{CaSiO}_3$ ,  $\text{Ca}_2\text{SiO}_4$  and bustamite (Bu,  $\text{CaMnSi}_2\text{O}_6$ ), which can be seen in Figure 8b–d. These reactions also resulted in the formation of water-soluble  $\text{MnCl}_2$  (Figure 7), which can be represented by Equations (10)–(12). By comparing the XRD patterns as shown in Figure 8b–d, the peaks for MnO became weaker with the increase of  $\text{CaCl}_2$  addition, confirming the presence of these reactions.





**Figure 7.** Recovery rates of elements by water-leaching the solid products vs. the addition of various amounts of CaCl<sub>2</sub> before carbothermic reduction.

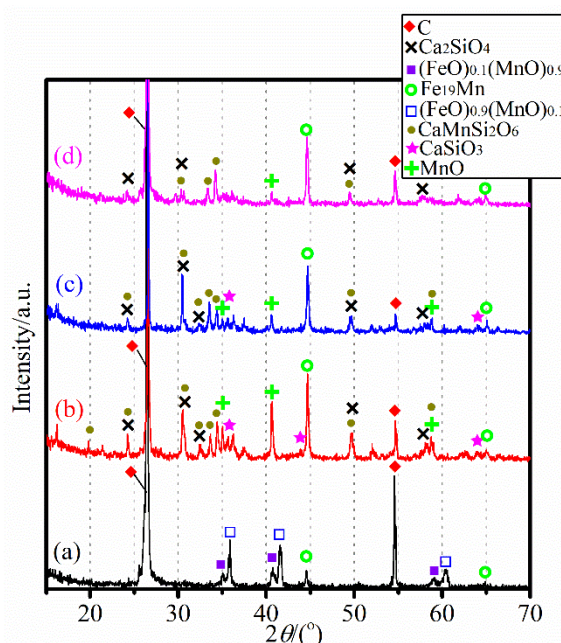


**Figure 8.** XRD patterns of the residues from water-leaching the products after reduction with addition of various amounts of CaCl<sub>2</sub> (a, 0 wt%; b, 10 wt%; c, 20 wt%; d, 30 wt%).

In the absence of CaCl<sub>2</sub>, carbothermic reduction was slow, forming monoxides of (FeO)<sub>0.9</sub>(MnO)<sub>0.1</sub>, (FeO)<sub>0.1</sub>(MnO)<sub>0.9</sub> and minor amounts of metallic Fe (i.e., Fe<sub>19</sub>Mn), as seen from Figure 8a. By comparison, the presence of CaCl<sub>2</sub> greatly accelerated the carbothermic reduction, revealed by the absence of Fe-bearing oxides and the sharp increase in the content of metallic Fe in the products (Figure 8b–d). In fact, selective near-complete reduction of Fe species has taken place in the presence of CaCl<sub>2</sub>, evidenced by both SEM and XRD analyses. In addition, the presence of CaCl<sub>2</sub> also promoted the formation of relatively large metallic Fe particles, which is advantageous in terms of subsequent liberation and magnetic/gravitational separation of metallic Fe from unwanted gangue. As an example, Figure 9 illustrates BSE micrograph and elemental mappings of the reduced product (after water-leaching) with 20 wt% CaCl<sub>2</sub> addition. As seen, the sizes of metallic Fe particles are generally in the range of 100–200 μm, which are much larger comparing to those formed in the absence of CaCl<sub>2</sub> (e.g., <40 μm as shown in Figure 6b, with 4 h reduction). The promoting effects of CaCl<sub>2</sub> addition on carbothermic reduction of Mn ore observed in the study was similar to that revealed during CaCl<sub>2</sub>-assisted carbothermic reduction of chromite ore [28,29], indicating a similar role played

in the reduction process.  $\text{CaCl}_2$  became molten at the reduction temperature of  $1000\text{ }^\circ\text{C}$ , because its melting point is  $775\text{ }^\circ\text{C}$  [33]. It is suggested that the presence of molten  $\text{CaCl}_2$  during reduction significantly promoted the segregation and transport of divalent and trivalent Fe from the oxides to the carbonaceous particles where further reduction took place, resulting in the formation of metallic Fe.

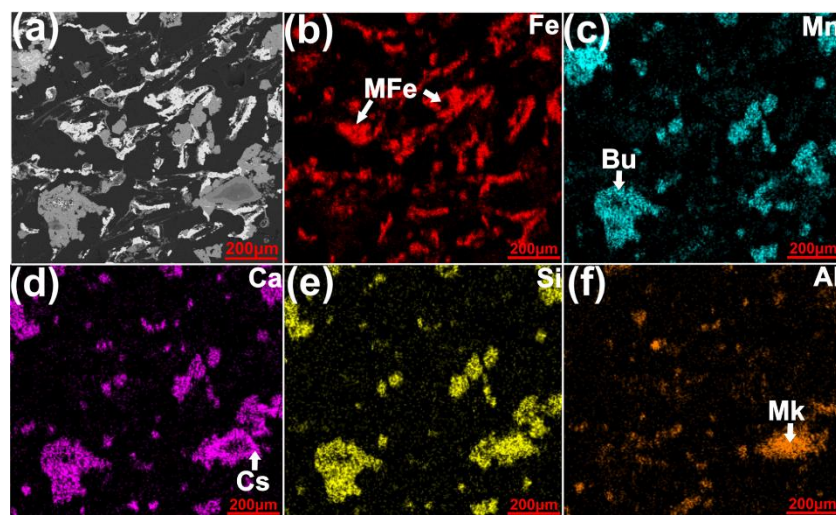


**Figure 9.** BSE image (a) and elemental mapping (b–f) of the reduced product (after water-leaching) with 20 wt%  $\text{CaCl}_2$  addition (MFe: metallic Fe; Bu: bustamite,  $\text{CaMnSi}_2\text{O}_6$ ; Cs: a Cl-bearing calcium aluminosilicate; Mk: metakaolin,  $\text{Al}_2\text{Si}_2\text{O}_7$ ).

As shown in Figure 9, in addition to the presence of significant amounts of bustamite produced by Equation (12), a metakaolin (Mk,  $\text{Al}_2\text{Si}_2\text{O}_7$ ) particle was also found that was surrounded by a shell of Cl-bearing calcium aluminosilicate (Cs), resulting from the reaction(s) involving  $\text{CaCl}_2$ .

### 3.4. Influence of $\text{MgCl}_2$ Addition

Carbothermic reduction of high-iron manganese ore was further conducted at  $1000\text{ }^\circ\text{C}$  for 2 h with the addition of 20 wt%  $\text{CaCl}_2$  and varying amounts of  $\text{MgCl}_2$  (0–60 wt% of the ore), aiming to selectively chlorinate the Mn species from the ore, while achieving selective metallization of Fe species. Degrees of chlorination and evaporation of chlorides for various elements were quantified (see Section 2.2) and plotted in Figures 10 and 11, respectively. It is obvious that  $\text{MgCl}_2$  was an effective chlorinating agent for the generation of water-soluble  $\text{MnCl}_2$ . Higher degrees of chlorination for Mn were achieved with the addition of higher amounts of  $\text{MgCl}_2$ . At 40 wt%  $\text{MgCl}_2$  addition, as much as 79.8 wt% Mn was chlorinated, with minimal Fe chlorination of as little as 2.8 wt%, demonstrating that selective Mn chlorination could be achieved. This is in excellent agreement with the thermodynamic predictions as discussed previously (see Section 1). Significant amounts of  $\text{MgCl}_2$  would remain in the reduced product when its addition was higher than 40 wt%. The presence of excessive  $\text{MgCl}_2$  would lead to progressive chlorination of Fe, reaching as high as 21.7% Fe chlorination with the addition of 60 wt%  $\text{MgCl}_2$ . Mn chlorination degree remained roughly the same, compared to that of 40 wt% addition. In addition, nearly 100% Ca remained water-soluble with the addition of  $\geq 20$  wt%  $\text{MgCl}_2$ , indicating that the 20 wt%  $\text{CaCl}_2$  added in the beginning did not contribute to the chlorination (Equations (10)–(12)). This is advantageous in terms of complete recovering  $\text{CaCl}_2$  from the product simply with water-leaching.

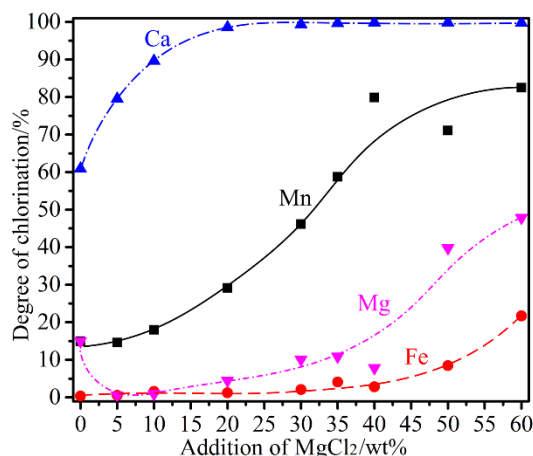


**Figure 10.** Degree of chlorination vs. the addition of various amounts of  $\text{MgCl}_2$  and 20 wt%  $\text{CaCl}_2$  before carbothermic reduction.

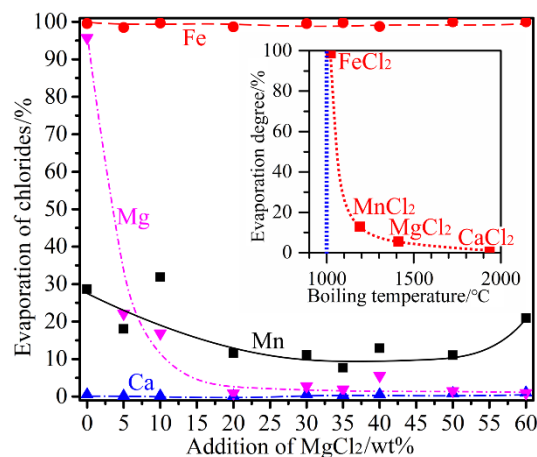


**Figure 11.** Evaporation degree of metal chlorides vs. the addition of various amounts of  $\text{MgCl}_2$  and 20 wt%  $\text{CaCl}_2$  before carbothermic reduction. Inset illustrates the correlation between the evaporation degree of divalent metal chlorides at 40 wt%  $\text{MgCl}_2$  addition and their respective boiling temperatures (boiling temperatures cited from reference [33]).

From Figure 11, it is seen that nearly 100% iron chloride became evaporated, while  $\text{CaCl}_2$  did not evaporate. The evaporation rate of  $\text{MnCl}_2$  was in the range of approximately 10–30%, depending on the addition of  $\text{MgCl}_2$ . Direct correlation between the evaporation rate of metal chlorides (at 40 wt%  $\text{MgCl}_2$  addition) and their boiling temperature (cited from reference [33]) can be observed from the inset of Figure 11, which is fundamentally determined by their equilibrium vapor pressures at the reduction temperature employed under the investigation (i.e., 1000 °C). As seen, metal chloride having a lower boiling temperature exhibited a higher evaporation rate. For example,  $\text{FeCl}_2$  has a boiling temperature of 1023 °C, indicating that its equilibrium vapor pressure is close to one atmospheric pressure during reduction at 1000 °C, resulting in its high evaporation rate of 98.7%. These results indicate that the difference between the evaporation rates of  $\text{FeCl}_2$  and  $\text{MnCl}_2$  could potentially be explored for their separation, and subsequent purification of  $\text{MnCl}_2$ .

In order to reveal the chlorination mechanism in the presence of  $\text{MgCl}_2$ , the sample products (after water-leaching) were subjected to XRD analysis (Figure 12). As seen from Figure 12, the addition of  $\text{MgCl}_2$  can effectively suppress the formation of Ca-bearing oxides (i.e.,  $\text{CaSiO}_3$ ,  $\text{Ca}_2\text{SiO}_4$ , and  $\text{CaMnSi}_2\text{O}_6$ ), which were produced from Equations (10)–(12). This was due to the occurrence and gradual domination of competing reactions consuming  $\text{SiO}_2$ , with the increase of  $\text{MgCl}_2$  addition. Furthermore, XRD results suggest that the presence of Mg-bearing oxides was in the form of  $\text{MgMnSiO}_4$

(at 10 and 20 wt%  $\text{MgCl}_2$  addition),  $\text{Mg}_2\text{SiO}_4$  (at 30–50 wt%  $\text{MgCl}_2$  addition), and  $\text{MgO}$  (at 30–50 wt%  $\text{MgCl}_2$  addition). Therefore, the main chlorination reactions involving  $\text{MgCl}_2$  can be deduced, and are represented as Equations (13)–(16). In the presence of both  $\text{CaCl}_2$  and  $\text{MgCl}_2$ ,  $\text{SiO}_2$  was preferably consumed by Equations (13) and (14), which dominated over Equations (10)–(12), suggesting a much stronger chlorination potential exerted by  $\text{MgCl}_2$  compared to  $\text{CaCl}_2$ . Increasing addition of  $\text{MgCl}_2$  would lead to the dominance of direct chlorination by  $\text{MgCl}_2$  (i.e., without the involvement of  $\text{SiO}_2$ ), which is represented by Equation (15). With the addition of >40 wt%  $\text{MgCl}_2$  addition, excessive  $\text{MgCl}_2$  started to chlorinate  $\text{FeO}$  (Equation (16)), resulting in the formation of water-soluble  $\text{FeCl}_2$  (Figure 10).

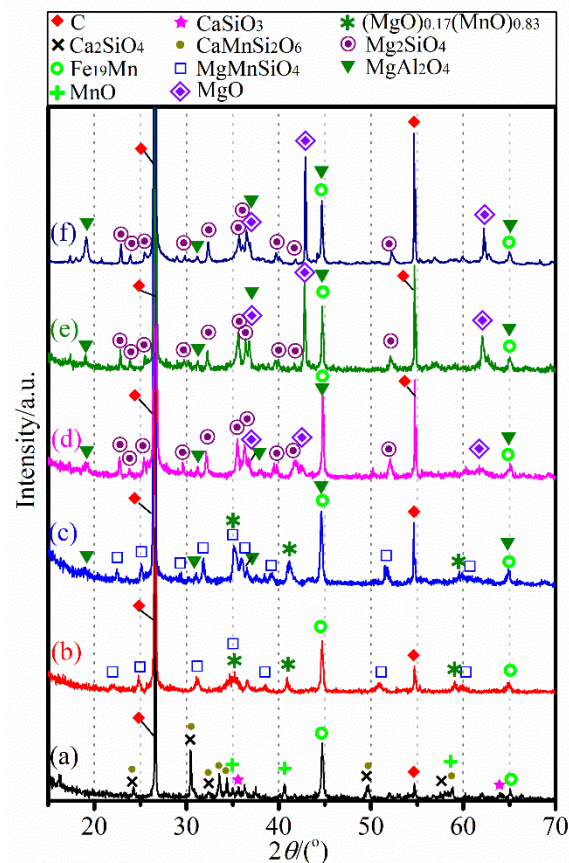
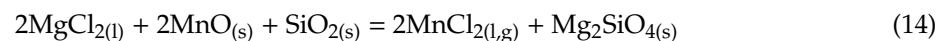
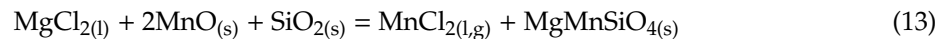


**Figure 12.** XRD patterns of the residues from water-leaching the products after reduction with the addition of 20 wt%  $\text{CaCl}_2$  and various amounts of  $\text{MgCl}_2$  (a, 0 wt%; b, 10 wt%; c, 20 wt%; d, 30 wt%; e, 40 wt%; f, 50 wt%).

Figure 13a exhibits the BSE image of the cross section of the product (after water-leaching) from carbothermic reduction in the presence of 20 wt%  $\text{CaCl}_2$  and 40 wt%  $\text{MgCl}_2$ . Formation of relatively large metallic Fe particles can be observed, resulting from the segregation effect due to presence of  $\text{CaCl}_2$  (see Section 3.3). Undissolved manganese was mainly in the form of binary monoxide  $(\text{MgO})_x(\text{MnO})_{1-x}$  containing minor amounts of  $\text{MgO}$ . Figure 13b–g shows the BSE image and elemental mappings of a particle characteristic of a core-shell structure. The core is porous polycrystalline

monoxide  $(\text{MgO})_x(\text{MnO})_{1-x}$  phase, which is surrounded by a layer of olivine-type  $\text{Mg}_{2-x}\text{Mn}_x\text{SiO}_4$  containing minor amounts of Mn. This suggests that inner diffusion of  $\text{Mg}^{2+}$  and outer diffusion of  $\text{Mn}^{2+}$  have taken place during chlorination.

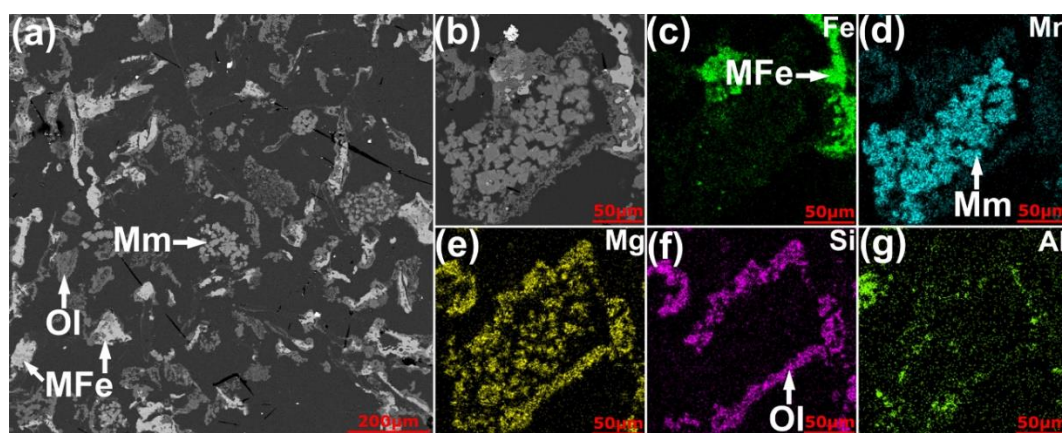


**Figure 13.** BSE image (a) of the reduced product (after water-leaching) with 20 wt%  $\text{CaCl}_2$  and 40 wt%  $\text{MgCl}_2$  addition at low magnification, and BSE image (b) of an individual reduced ore particle with its elemental mapping graphs (c–g) MFe: metallic Fe; Mm:  $(\text{MgO})_x(\text{MnO})_{1-x}$ ; Ol: olivine-type  $\text{Mg}_{2-x}\text{Mn}_x\text{SiO}_4$ .

### 3.5. Influence of Reaction Time

With the addition of 20 wt%  $\text{CaCl}_2$  and 40 wt%  $\text{MgCl}_2$ , carbothermic reduction of Mn ore was conducted with the variation of dwelling time (0–4 h) at 1000 °C. Degrees of chlorination and the evaporation rate of chlorides were determined (Figures 14 and 15). It is seen that chlorination of Mn species was fast, suggested by the chlorination degree of 70.8% achieved at 0 h. It should be noted that this particular test was conducted by heating at 15 °C/min to 1000 °C, followed by immediate cooling at 15 °C/min without dwelling at 1000 °C (i.e., 0 h at 1000 °C). Therefore, chlorination reactions taking place during heating and cooling periods accounted for the 70.8% Mn chlorination. After dwelling at 1000 °C for 1 h, the Mn chlorination degree reached 89.4%. Further increase in the dwelling time did not lead to improvement in Mn chlorination. Chlorination degrees of Ca, Mg and Fe retained at relatively constant values (i.e., 99.8%, 5.2%, and 3.1%, respectively), irrespective of the dwelling time. In contrast, the dwelling time had a greater influence on the evaporation of chlorides, which can be seen from Figure 15. As little as only 17.0%  $\text{FeCl}_2$  evaporated with 0 h dwelling time, which increased dramatically to 98.5% after dwelling at 1000 °C for 1 h. This can be explained by the much higher vapor pressure of  $\text{FeCl}_2$  at 1000 °C, leading to its near-complete evaporation. Increase in the evaporation of  $\text{MnCl}_2$  and  $\text{MgCl}_2$  can also be observed with prolonged dwelling.

After prolonged dwelling for 4 h, the main phases after water-leaching are metallic Fe, magnesia  $\text{MgO}$ , olivine-type  $\text{Mg}_{2-x}\text{Mn}_x\text{SiO}_4$ , and minor amounts of magnesio-aluminosilicate (i.e., pyrope,  $\text{Mg}_3\text{Al}_2(\text{SiO}_4)_3$ ), based on SEM (Figure 16) and XRD analyses. As seen from Figure 16, Metallic Fe particles are relatively large, with their particle sizes generally in the range of 100–200 μm.  $\text{MgO}$  particles are smaller in size, measuring less than 50 μm.

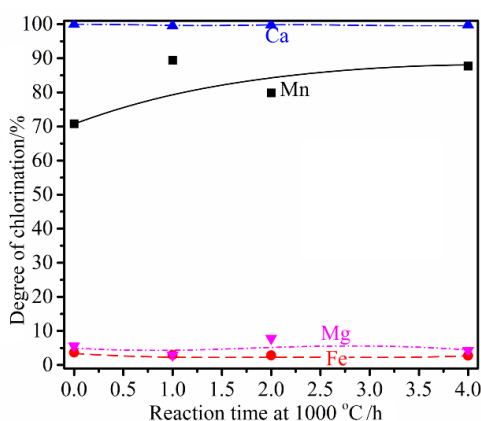


**Figure 14.** Degree of chlorination vs. reaction time at 1000 °C with the addition of 20 wt% CaCl<sub>2</sub> and 40 wt% MgCl<sub>2</sub>.

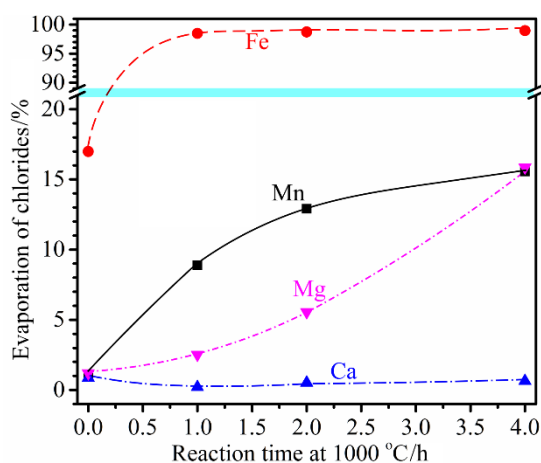


**Figure 15.** Evaporation degrees of metal chlorides vs. reaction time at 1000 °C with the addition of 20 wt% CaCl<sub>2</sub> and 40 wt% MgCl<sub>2</sub>.

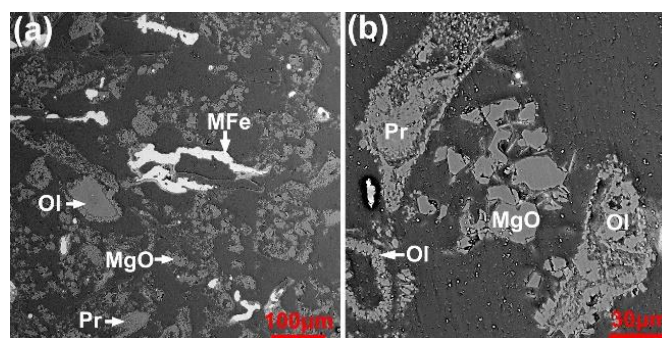


**Figure 16.** BSE images (a,  $\times 450$ ; b,  $\times 1750$ ) of the reduced product (after water-leaching) from reduction with the addition of 20 wt% CaCl<sub>2</sub> and 40 wt% MgCl<sub>2</sub> at 1000 °C for 4 h (MFe: metallic Fe; Ol: olivine-type Mg<sub>2-x</sub>Mn<sub>x</sub>SiO<sub>4</sub>; Pr: pyrope, Mg<sub>3</sub>Al<sub>2</sub>(SiO<sub>4</sub>)<sub>3</sub>).

### 3.6. Influence of the Presence of Water

The influence of the presence of water was also investigated by pre-mixing the ore with 18 wt% graphite, 20 wt% CaCl<sub>2</sub>, 40 wt% MgCl<sub>2</sub> and varying amounts of water (0–10 wt% of the ore), followed by heating at 1000 °C for 2 h. The degrees of chlorination were quantified, and plotted in Figure 17a. It is obvious that the presence of water was detrimental to the chlorination of Mn species from the ore, evidenced by a significant decrease of Mn chlorination from 79.8% to 46.3% in the presence of 10 wt%

water. This was likely due to the consumption of the chlorinating agent  $\text{MgCl}_2$  by  $\text{H}_2\text{O}$  when heated, which can be represented by Equation (17). The resulting gaseous  $\text{HCl}$  would evolve quickly from the sample mixture and be carried away by the purging Ar gas, before effective chlorination of the ore took place. Furthermore, it appears that less amounts of metallic Fe have formed (Figure 17b) with the addition of water, compared to the case without water addition (Figure 13).

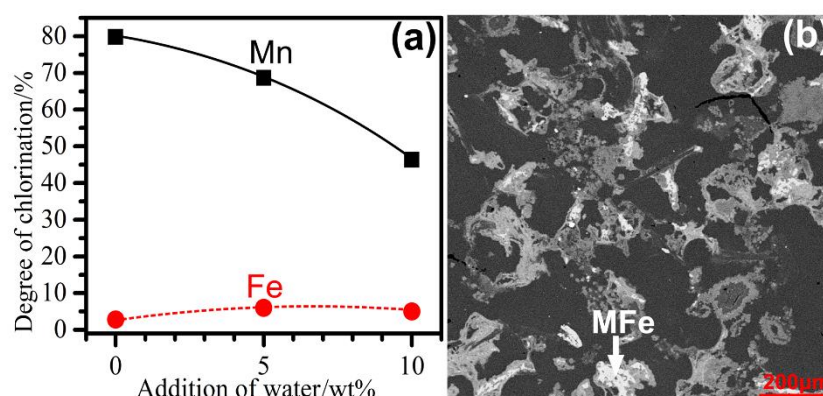
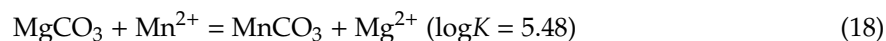


**Figure 17.** (a) Recovery Mn and Fe by water-leach from solid products following reduction at 1000 °C with the addition of 20 wt%  $\text{CaCl}_2$ , 40 wt%  $\text{MgCl}_2$  and varying amounts of water, and (b) BSE image of the reduced product with the addition of 10 wt% water (MFe: metallic Fe).

### 3.7. Proposed Flow Sheet

Based on the experimental results, the flow sheet for the processing of high-Fe manganese ore was tentatively suggested, which is shown in Figure 18. With the addition of 18 wt% graphite as the carbonaceous reductant, 20 wt%  $\text{CaCl}_2$  and 40 wt%  $\text{MgCl}_2$  as the chlorination agent, simultaneous selective chlorination and carbothermic reduction of high-iron manganese ore can be achieved after reduction at 1000 °C for 1 h. As much as 89.4% of Mn can be recovered by water-leaching the product, with minimal dissolution of only 3.0% Fe. The leach residue contains relatively large metallic Fe particles, which can be effectively recovered by magnetic separation. Bearing high concentrations of  $\text{Mn}^{2+}$ ,  $\text{Ca}^{2+}$ , and minor amounts of  $\text{Fe}^{2+}$ , the leachate can be treated with carbonate precipitation after iron removal, for the precipitation and recovery of  $\text{Mn}^{2+}$  in the form of  $\text{MnCO}_3$ . Selective carbonate precipitation of  $\text{Mn}^{2+}$  with the addition of  $\text{MgCO}_3$  is possible at a pH of approximately 8.5, indicated by Equations (18) and (19) [34]. Equation (19) suggests that, during the carbonate precipitation of  $\text{Mn}^{2+}$  from the solution,  $\text{Ca}^{2+}$  would not co-precipitate (in the form of  $\text{CaCO}_3$ ), as long as the concentration of  $\text{Mn}^{2+}$  is still higher than 1/224 of the  $\text{Ca}^{2+}$  concentration, determined by the equilibrium constant  $K$ . Preliminary experiments on the selective carbonate precipitation were conducted, confirming its feasibility.



The solution produced from carbonate precipitation would be enriched in  $\text{MgCl}_2$  and  $\text{CaCl}_2$ , both of which can be recovered in their solid form for re-use (Figure 18), thereby significantly lowering the material cost of the proposed process. Theoretically,  $\text{MgCl}_2$  and  $\text{CaCl}_2$  can be completely recycled within the process without any consumption. The overall process would only require the input of carbonaceous reductant and  $\text{MgCO}_3$ , in addition to the ore, producing high purity  $\text{MnCO}_3$  and metallic Fe powders. This represents an innovative and cost-effective approach for the processing of high-Fe manganese ores in an environmentally friendly manner.

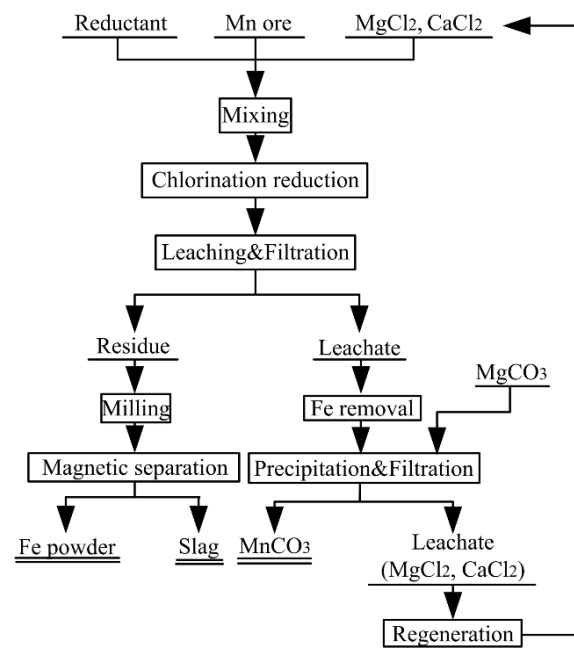


**Figure 18.** Proposed flow sheet for the selective chlorination and carbothermic reduction of high-Fe manganese ore.

#### 4. Conclusions

Aiming at achieving selective chlorination of Mn and selective metallization of Fe in a simultaneous manner, the high-Fe manganese ore was reduced using graphite powders at 1000 °C in the presence of CaCl<sub>2</sub> and MgCl<sub>2</sub>. Based on the experimental results, the following can be concluded.

- (1) Simultaneous chlorination of Mn and metallization of Fe from the high-Fe manganese ore is feasible. With the addition of 18 wt% graphite as the carbonaceous reductant, 20 wt% CaCl<sub>2</sub> and 40 wt% MgCl<sub>2</sub> as the chlorinating agent, heating the manganese ore at 1000 °C for 1 h resulted in the selective chlorination of Mn reaching as much as 89.4%, with the Fe chlorination of only 3.0%. Most Fe oxides in the ore were reduced to the metallic form, with the particle sizes generally in the range of 100–200 μm, allowing subsequent easier separation and upgrading of the metallic Fe particles.
- (2) The presence of CaCl<sub>2</sub> greatly accelerated the selective reduction of Fe oxides to their metallic form. In addition, it promoted the formation of relatively large metallic Fe particles, facilitating their subsequent separation. In the absence of MgCl<sub>2</sub>, CaCl<sub>2</sub> alone could selectively chlorinate Mn only to a limited degree. The chlorination involved reacting with quartz which was present in the Mn ore as gangue, forming calcium silicates and MnCl<sub>2</sub> (Equations (10)–(12)).
- (3) MgCl<sub>2</sub> was a stronger chlorinating agent comparing to CaCl<sub>2</sub>. Selective chlorination of Mn to a high degree was possible in the presence of MgCl<sub>2</sub>, in which case the presence of CaCl<sub>2</sub> did not contribute to the chlorination. However, addition of excessive amounts of MgCl<sub>2</sub> would lead to gradual increase in the chlorination of Fe without further improving the Mn chlorination degree. Chlorination using MgCl<sub>2</sub> would preferably involve reacting with quartz forming magnesium silicates and MnCl<sub>2</sub> Equations (13) and (14). Once the quartz was consumed completely, direct chlorination of MnO by MgCl<sub>2</sub> would take place (Equation (15)).
- (4) The presence of water was detrimental to the selective chlorination of Mn from the ore, likely due to the presence of HCl-generating reaction (Equation (17)) competing for MgCl<sub>2</sub>.

**Supplementary Materials:** The following are available online at <http://www.mdpi.com/2075-4701/9/10/1124/s1>.

**Author Contributions:** D.Y. conceived and designed the experiments; F.C., Y.C., and C.Z. performed the experiments; D.Y., X.G., and Q.T. analyzed the data; D.Y. wrote the paper; D.Y., X.G., and Q.T. contributed to the funding acquisition.

**Funding:** This research was funded by National Natural Science Foundation of China, grant number 51904350, grant number 51922108, Hunan Natural Science Foundation, grant number 2019JJ20031, and the startup fund of the Central South University.

**Acknowledgments:** The authors thank Jiabin Wang of the Changsha Research Institute of Mining and Metallurgy Co., Ltd. for providing the manganese ore. The authors also thank Zhengqi Guo of the School of Minerals Processing and Bioengineering, Central South University, for helping with the crushing and grinding of the manganese ore.

**Conflicts of Interest:** The authors declare no conflict of interest.

## References

1. Singh, V.; Biswas, A. Physicochemical processing of low grade ferruginous manganese ores. *Int. J. Miner. Process.* **2017**, *158*, 35–44. [[CrossRef](#)]
2. Pagnanelli, F.; Garavini, M.; Vegliò, F.; Toro, L. Preliminary screening of purification processes of liquor leach solutions obtained from reductive leaching of low-grade manganese ores. *Hydrometallurgy* **2004**, *71*, 319–327. [[CrossRef](#)]
3. Hagelstein, K. Globally sustainable manganese metal production and use. *J. Environ. Manag.* **2009**, *90*, 3736–3740. [[CrossRef](#)] [[PubMed](#)]
4. Yi, L.; Huang, Z.; Jiang, T.; Zhao, P.; Zhong, R.; Liang, Z. Carbothermic Reduction of Ferruginous Manganese Ore for Mn/Fe Beneficiation: Morphology Evolution and Separation Characteristic. *Minerals* **2017**, *7*, 167. [[CrossRef](#)]
5. Corathers, L.A. *USGS 2015 Minerals Yearbook-Manganese*; U.S. Geological Survey: Reston, VA, USA, 2019.
6. Kononov, R.; Ostrovski, O.; Ganguly, S. Carbothermal Solid State Reduction of Manganese Ores: 1. Manganese Ore Characterisation. *ISIJ Int.* **2009**, *49*, 1099–1106. [[CrossRef](#)]
7. Gao, Y.B.; Kim, H.G.; Sohn, H.Y. Kinetics of pre-reduction of manganese ore by CO. *Min. Process. Extr. Met.* **2012**, *121*, 109–116. [[CrossRef](#)]
8. Akdogan, G.; Eric, R.H. Kinetics of the solid-state carbothermic reduction of wessel manganese ores. *Met. Mater. Trans. B* **1995**, *26*, 13–24. [[CrossRef](#)]
9. Abdel Halim, K.S.; Bahgat, M.; Morsi, M.B.; El-Barawy, K. Pre-reduction of manganese ores for ferromanganese industry. *Ironmak. Steelmak.* **2011**, *38*, 279–284. [[CrossRef](#)]
10. Braga, R.S.; Takano, C.; Mourão, M.B. Prereduction of self-reducing pellets of manganese ore. *Ironmak. Steelmak.* **2007**, *34*, 279–284. [[CrossRef](#)]
11. Zhang, W.; Cheng, C.Y. Manganese metallurgy review. Part I: Leaching of ores/secondary materials and recovery of electrolytic/chemical manganese dioxide. *Hydrometallurgy* **2007**, *89*, 137–159. [[CrossRef](#)]
12. Zhang, C.; Wang, S.; Cao, Z.F.; Zhong, H. Recovery of manganese from manganese oxide ores in the EDTA solution. *Met. Res. Technol.* **2018**, *115*, 306. [[CrossRef](#)]
13. Acharya, C.; Kar, R.N.; Sukla, L.B. Studies on reaction mechanism of bioleaching of manganese ore. *Min. Eng.* **2003**, *16*, 1027–1030. [[CrossRef](#)]
14. Mpho, M.; Samson, B.; Ayo, A. Evaluation of reduction roasting and magnetic separation for upgrading Mn/Fe ratio of fine ferromanganese. *Int. J. Min. Sci. Technol.* **2013**, *23*, 537–541. [[CrossRef](#)]
15. You, Z.; Li, G.; Zhang, Y.; Peng, Z.; Jiang, T. Extraction of manganese from iron rich MnO<sub>2</sub> ores via selective sulfation roasting with SO<sub>2</sub> followed by water leaching. *Hydrometallurgy* **2015**, *156*, 225–231. [[CrossRef](#)]
16. Paixdo, J.M.M.; Amaral, J.C.; Memória, L.E.; Freitas, L.R. Sulphation of Carajás manganese ore. *Hydrometallurgy* **1995**, *39*, 215–222. [[CrossRef](#)]
17. Zhang, Y.; You, Z.; Li, G.; Jiang, T. Manganese extraction by sulfur-based reduction roasting–acid leaching from low-grade manganese oxide ores. *Hydrometallurgy* **2013**, *133*, 126–132. [[CrossRef](#)]
18. Zhang, Y.B.; Zhao, Y.; You, Z.X.; Duan, D.X.; Li, G.H.; Jiang, T. Manganese extraction from high-iron-content manganese oxide ores by selective reduction roasting–acid leaching process using black charcoal as reductant. *J. Cent. South Univ.* **2015**, *22*, 2515–2520. [[CrossRef](#)]
19. Zhao, Y.; Zhu, G.; Cheng, Z. Thermal analysis and kinetic modeling of manganese oxide ore reduction using biomass straw as reductant. *Hydrometallurgy* **2010**, *105*, 96–102. [[CrossRef](#)]

20. Zhang, H.; Zhu, G.; Yan, H.; Li, T.; Feng, X. Thermogravimetric Analysis and Kinetics on Reducing Low-Grade Manganese Dioxide Ore by Biomass. *Met. Mater. Trans. B* **2013**, *44*, 878–888. [[CrossRef](#)]
21. Zhang, H.; Zhu, G.; Yan, H.; Zhao, Y.; Li, T.; Feng, X. Reduction of low-grade manganese dioxide ore pellets by biomass wheat stalk. *Acta Met. Sin. (Engl. Lett.)* **2013**, *26*, 167–172. [[CrossRef](#)]
22. Long, Y.F.; Su, J.; Ye, X.J.; Su, H.F.; Wen, Y.X. Reduction-Roast Leaching of Low-Grade Pyrolusite Using Bagasse as a Reducing Agent. *Adv. Mater. Res.* **2013**, *699*, 28–33. [[CrossRef](#)]
23. Cheng, Z.; Zhu, G.; Zhao, Y. Study in reduction-roast leaching manganese from low-grade manganese dioxide ores using cornstalk as reductant. *Hydrometallurgy* **2009**, *96*, 176–179. [[CrossRef](#)]
24. Sharma, T. Physico-chemical processing of low grade manganese ore. *Int. J. Miner. Process.* **1992**, *35*, 191–203. [[CrossRef](#)]
25. Sinha, M.K.; Purcell, W. Reducing agents in the leaching of manganese ores: A comprehensive review. *Hydrometallurgy* **2019**, *187*, 168–186. [[CrossRef](#)]
26. Gao, Y.; Olivias-Martinez, M.; Sohn, H.Y.; Kim, H.G.; Kim, C.W. Upgrading of Low-Grade Manganese Ore by Selective Reduction of Iron Oxide and Magnetic Separation. *Met. Mater. Trans. B* **2012**, *43*, 1465–1475. [[CrossRef](#)]
27. Wu, Y.; Shi, B.; Ge, W.; Yan, C.J.; Yang, X. Magnetic Separation and Magnetic Properties of Low-Grade Manganese Carbonate Ore. *JOM* **2015**, *67*, 361–368. [[CrossRef](#)]
28. Yu, D.; Paktunc, D. Calcium Chloride-Assisted Segregation Reduction of Chromite: Influence of Reductant Type and the Mechanism. *Minerals* **2018**, *8*, 45. [[CrossRef](#)]
29. Yu, D.; Paktunc, D. Direct Production of Ferrochrome by Segregation Reduction of Chromite in the Presence of Calcium Chloride. *Metals* **2018**, *8*, 69. [[CrossRef](#)]
30. Roine, A. *HSC Chemistry*; Outokumpu Research Oy: Pori, Finland, 2007.
31. Boudouard, M.O. Recherches sur les equilibres chimiques. *Ann. Chim. Phys.* **1901**, *24*, 1–85.
32. Yu, D.; Zhu, M.; Utigard, T.A.; Barati, M. TG/DTA study on the carbon monoxide and graphite thermal reduction of a high-grade iron nickel oxide residue with the presence of siliceous gangue. *Thermochim. Acta* **2014**, *575*, 1–11. [[CrossRef](#)]
33. Lide, D.R. *CRC Handbook of Chemistry and Physics, Internet Version 2005*; CRC Press: Boca Raton, FL, USA, 2005.
34. Zhang, W.; Cheng, C.Y. Manganese metallurgy review. Part II: Manganese separation and recovery from solution. *Hydrometallurgy* **2007**, *89*, 160–177. [[CrossRef](#)]



© 2019 by the authors. Licensee MDPI, Basel, Switzerland. This article is an open access article distributed under the terms and conditions of the Creative Commons Attribution (CC BY) license (<http://creativecommons.org/licenses/by/4.0/>).